Passive Electromagnetic Field Positioning Method Based on BP Neural Network in Underwater 3-D Space

Chaoyi Wang[1], Yidong Xu[1,3(✉)], Junwei Qi[1], Wenjing Shang[1], Mingxin Liu[1], and Wenjian Chen[2]

[1] College of Information and Communication Engineering, Harbin Engineering University, Harbin 150001, China
xuyidong@hrbeu.edu.cn
[2] College of Underwater Acoustic Engineering, Harbin Engineering University, Harbin 150001, China
[3] Yantai Research Institute of Harbin Engineering University, Yantai 264000, China

Abstract. This paper studies the positioning method of combining the passive electric field positioning and passive magnetic field positioning under three-dimensional (3-D) water. This technology can be applied to underwater submarine positioning, underwater leakage power supply positioning, underwater rescue and other occasions. We collect the samples data by electromagnetic sensors array, and recover the location of the targets. After the data preprocessing process includes data normalization, de-redundancy process, and generalization process, we use Back Propagation (BP) neural networks to build electric field and magnetic field distribution models of electric dipole source. Finally, we enter the test data to obtain the target position in the well-trained positioning model. We take the Euclidean distance between the ideal position and the model output target position as an absolute error. The results show that this method can effectively improve the accuracy of underwater target positioning and anti-interference ability of the training model, and the nonlinear function model trained by the neural network can be applied to the complex and changeable underwater environment.

Keywords: BP neural networks · Passive positioning · Anti-interference

This research work was supported by International Science & Technology Cooperation Program of China (2014DFR10240), the Fundamental Research Funds for the Central Universities (3072021CF0802), the Key Laboratory of Advanced Marine Communication and Information Technology, Ministry of Industry and Information Technology (AMCIT2101-02), and Sino-Russian Cooperation Fund of Harbin Engineering University (2021HEUCRF006).

S. Liu and X. Ma (Eds.): ADHIP 2021, LNICST 416, pp. 292–304, 2022.
https://doi.org/10.1007/978-3-030-94551-0_24

1 Introduction

With the development and enrichment of underwater electric and magnetic sensor technology, the acquisition accuracy and acquisition speed of the sensors have been greatly improved, and the conditions of data acquisition device can gradually meet the requirements of theoretical experiments. Research on passive positioning of underwater targets has also attracted more and more attention from scientific researchers [1]. This technology is widely used in underwater rescue, underwater exploration and maintenance of flooded urban facilities. In practical applications, small data fluctuations may introduce huge errors, especially in the complex and changeable underwater environment. The adaptive weakening of underwater interference and nonlinear multi-parameter inversion methods are the main difficulties in this research direction.

Passive electric field positioning technology set electric dipole sources as targets that emits an electromagnetic field in an infinite homogeneous medium [2,3]. We studies the nonlinear mapping relationship between the position of the electric dipole source and electromagnetic field that it emits. Magnetic field data positioning has stronger anti-interference ability, but the magnetic field data is particularly weak and requires higher accuracy of the magnetic sensor [4–6]. Therefore, there is less research on passive magnetic field positioning technology.

We mainly study the method of combining passive electric field positioning and passive magnetic field positioning based on BP neural network. BP artificial neural network is suitable for training nonlinear mapping models. Our innovation lies in the use of electromagnetic field data for positioning of targets, and the use of neural networks to deal with nonlinear inversion problems. It uses forward model for data preprocessing, automatically configures weighting factors, and combines electric field data and magnetic field data to co-locate targets. Judging the weighting factors of training samples by interference strength, on one hand, can improve the adaptive adjustment ability of training parameters, and then improve the system's anti-interference ability in the complex and changeable underwater environment. On another hand, it can remove useless parameter information, reduce the burden of neural network training, and greatly improve training efficiency. Therefore, positioning models trained by BP neural network obtain anti-jamming capabilities and rapid positioning capabilities based on high accuracy.

2 Forward Model Derived from Theory

In an infinite uniform conductive medium, there is a nonlinear mapping relationship between the position $\mathbf{r}$ of the electric dipole source and the electromagnetic field data it emits. The electric potential difference U distribution model and the magnetic field intensity $\mathbf{H}$ distribution model derived from $\mathbf{r}$ are defined as forward models [7]. On the contrary, the process of obtaining $\mathbf{r}$ from U and $\mathbf{H}$ is defined as the inversion process, that is, the positioning process. The forward model provides reference samples for building a neural network model in the inversion process. It can extract effective information, remove redundant samples, and reduce computing space.

As shown in Fig. 1, in an infinite uniform conductive medium, we set the electric dipole source at the origin of the spherical coordinate system, the electric dipole moment is **p**, the electric field intensity **E** at point Q is $(E_r, E_\varphi, E_\theta)$, and the magnetic field intensity **H** at point Q is $(H_r, H_\varphi, H_\theta)$. Suppose the conductive medium is fresh water, the electric conductivity is σ, and the permittivity is ε. The electric dipole source radiates a DC signal, and the angular frequency of the signal is $\omega = 0$.

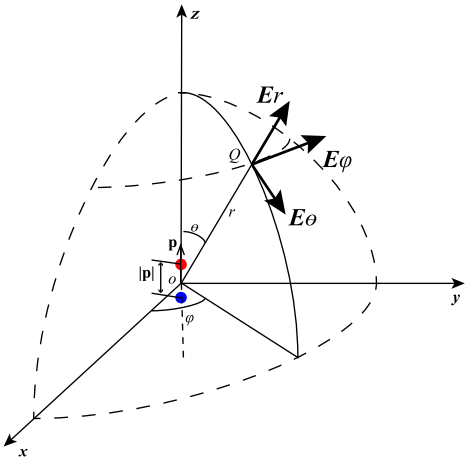

Fig. 1. Electric field distribution diagram of electric dipole source.

When $\sigma >> \omega\varepsilon$, under the spherical coordinate system, the radiant electromagnetic field of the DC electric dipole source is satisfied with the equation [8]:

$$E_r = \frac{|\mathbf{p}| \cos\theta}{2\pi\sigma r^3} \tag{1}$$

$$E_\theta = \frac{|\mathbf{p}| \sin\theta}{2\pi\sigma r^3} \tag{2}$$

$$H_\varphi = \frac{|\mathbf{p}| \sin\theta}{4\pi r^2} \tag{3}$$

Where $\mathbf{r} = (x, y, z)$, $r = |\mathbf{r}|$. Multiply $(E_r, E_\varphi, E_\theta)$ and $(H_r, H_\varphi, H_\theta)$ by the transition matrix. The transition matrix transitions from the spherical coordinate system to the rectangular coordinate system. Transform $(E_r, E_\varphi, E_\theta)$ and $(H_r, H_\varphi, H_\theta)$ into the expression of rectangular coordinate system:

$$E_x = \frac{3\,|\mathbf{p}|\, zx}{4\pi\sigma r^5} \tag{4}$$

$$E_y = \frac{3\,|\mathbf{p}|\, zy}{4\pi\sigma r^5} \tag{5}$$

$$E_z = \frac{3\,|\mathbf{p}|\,z^2}{4\pi\sigma r^5} - \frac{\mathbf{p}}{4\pi\sigma r^3\,|\mathbf{p}|} \tag{6}$$

$$H_x = \frac{-\,|\mathbf{p}|\,y}{4\pi r^3} \tag{7}$$

$$H_y = \frac{|\mathbf{p}|\,x}{4\pi r^3} \tag{8}$$

E can be deduced as:

$$\mathbf{E} = \frac{3(\mathbf{p} \bullet \mathbf{r})\mathbf{r} - r^2\mathbf{p}}{4\pi\sigma r^5} \tag{9}$$

In the actual measurement process, the data measured by the electric field sensor is the electric potential difference U. We need to transform **E** into U. Therefore, in an infinite uniform underwater environment, the forward model from the position information (**r** and **p**) to the electromagnetic field data (U and **H**) is:

$$U = \frac{\mathbf{p} \bullet \mathbf{r}}{4\pi\sigma r^3} \tag{10}$$

$$\mathbf{H} = (H_x, H_y, 0) \tag{11}$$

3 Data Preprocessing

3.1 Acquisition of Training Samples

We place 24 receiving array elements in an underwater 3-D space with a range of 100 m × 100 m × 30 m to form a sensor array [9]. Set the reference electrode of the electric sensors at the center of the array. Each array element is equipped with an electric sensor and a magnetic sensor to receive U and **H** respectively. In addition, we have arranged media that produce both electric and magnetic field disturbances as the sources of interference underwater. Because the conductivity and magnetic permeability of the media are different in strength, the disturbances caused by the media are biased magnetic field or biased electric field.

In an underwater environment where the signal-to-noise ratio (SNR) is 40 dB, after collecting N samples and normalizing them, the electric field training set $\mathbf{E}_{\mathrm{N}}$ and the magnetic field training set $\mathbf{M}_{\mathrm{N}}$ can be obtained. Where $\mathbf{E}_{\mathrm{N}}$ contains sample set $\mathbf{R}_{3\times\mathrm{N}}$ (Electric dipole position), $\mathbf{P}_{3\times\mathrm{N}}$ (electric dipole moment) and label set $\mathbf{U}_{24\times\mathrm{N}}$, $\mathbf{M}_{\mathrm{N}}$ contains sample set $\mathbf{R}_{3\times\mathrm{N}}$, $\mathbf{P}_{3\times\mathrm{N}}$ and label set $\mathbf{H}_{24\times\mathrm{N}}$.

3.2 De-redundancy and Generalization of Training Set

De-redundancy. The de-redundancy process can remove samples with large data deviations caused by the interferences in the measured area. We substitute $\mathbf{R}_{3\times\mathrm{N}}$ and $\mathbf{P}_{3\times\mathrm{N}}$ into the forward model of formulas (10), (11) to obtain the theoretical electromagnetic field data sets ($\mathbf{U}^{\mathrm{o}}{}_{24\times\mathrm{N}}$ and $\mathbf{H}^{\mathrm{o}}{}_{24\times\mathrm{N}}$). Next, we find the Euclidean distance $\mathbf{D}_{\mathrm{N}}$ of the column vectors between the theoretical set $\mathbf{U}^{\mathrm{o}}{}_{24\times\mathrm{N}}$ and the measurement set $\mathbf{U}_{24\times\mathrm{N}}$, and calculate the average value $\bar{D}$ of $\mathbf{D}_{\mathrm{N}}$. In this experiment, we removed the samples whose Euclidean distance is greater than $\bar{D}$ to obtain the new training set $\mathbf{E}_{\mathrm{S}}$ after de-redundancy. In the same way, after removing the magnetic samples with large interference, the new training set $\mathbf{M}_{\mathrm{T}}$ of the passive magnetic field positioning model is obtained.

Generalization. The process of de-redundancy may lead to non-uniform distribution of samples in the positioning area, which is manifested in the centralized distribution of data or missing data in individual areas. We solve such problems through a generalization process. The steps of generalization processing are as follows:

We cut the positioning area ($100\,\mathrm{m} \times 100\,\mathrm{m} \times 30\,\mathrm{m}$) into 25 sub-areas ($20\,\mathrm{m} \times 20\,\mathrm{m} \times 30\,\mathrm{m}$) through refinement processing. The number of samples in the i-th sub-area is defined as M_i, the maximum M_i in the 25 sub-areas is taken as $\mathrm{M}_{\max}$, and the minimum M_i is taken as $\mathrm{M}_{\min}$. We take the decision threshold as $a = (\mathrm{M}_{\max} + \mathrm{M}_{\min})/2$, and set the step size to $b = (\mathrm{M}_{\max} - \mathrm{M}_{\min})/2$.

The algorithm is used to traverse the samples in each sub-area. When judging $\mathrm{M}_i > a$, the training set samples in the i-th sub-area are sorted in ascending order, according to the Euclidean distance between the theoretical data and the measured data. The first b samples in this sub-area are removed to update the training set in this sub-area. When $\mathrm{M}_i > b$, keep the training set of this sub-area unchanged.

After generalization, the result shows that $\mathbf{E}_{\mathrm{S}}$ is updated to $\mathbf{E}_{\mathrm{K}}$, and the number of samples is K. $\mathbf{E}_{\mathrm{K}}$ includes sample set $\mathbf{U}_{24\times\mathrm{K}}$, label set $\mathbf{R}_{3\times\mathrm{K}}$, $\mathbf{P}_{3\times\mathrm{K}}$. We update $\mathbf{M}_{\mathrm{T}}$ to $\mathbf{M}_{\mathrm{L}}$ through the same steps, and the number of samples is L. $\mathbf{M}_{\mathrm{L}}$ is divided into sample set $\mathbf{H}_{24\times\mathrm{L}}$ and label set $\mathbf{R}_{3\times\mathrm{L}}$, $\mathbf{P}_{3\times\mathrm{L}}$ for training BP neural networks.

3.3 Weight Factors

The weight factors represent the ratio of the effective training data to the total training data in a certain sub-area. In the data sets $\mathbf{E}_{\mathrm{K}}$ and $\mathbf{M}_{\mathrm{L}}$, the number of updated samples in the i-th sub-area is K_i and L_i. We define the weight factor of $\mathbf{E}_{\mathrm{K}}$ in the i-th sub-area as $\alpha_i = \mathrm{K}_i/(\mathrm{K}_i + \mathrm{L}_i)$, and the weight factor of $\mathbf{M}_{\mathrm{L}}$ in the i-th sub-area as $\beta_i = \mathrm{K}_i/(\mathrm{K}_i + \mathrm{L}_i)$. The conductivity and magnetic permeability of the interference source are different in strength. The weight factors can judge the credibility of the electric field model [10,11] and the magnetic field model by proportion of the effective samples in the interference area, so as to allocate the proportion of the outputs from the electric field model and the magnetic field model, improve the accuracy and anti-interference ability of the positioning model.

4 Inversion Model Trained by BP Neural Network

Research shows that the training accuracy of BP neural network is not greatly affected by the number of layers. As long as the number of neurons in the hidden layer is large enough, a single hidden layer can also approximate a nonlinear function model with finite discontinuities in arbitrary accuracy. Therefore, we choose a single hidden layer BP neural network to train the passive electric field model and passive magnetic field positioning model.

4.1 Passive Electric Field Positioning Model (E-model) and Passive Magnetic Field Positioning Model (H-model)

The BP neural network for training E-model and H-model has three layers, namely the input layer, the hidden layer and the output layer (Fig. 2).

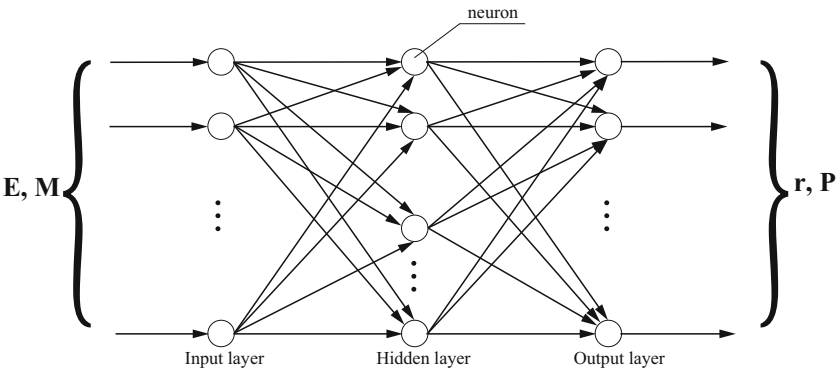

Fig. 2. The structure of BP neural network.

For E-model, characteristic parameters' number of the input layer is 24, and the number of samples is K. The number of neurons in the hidden layer is set to 240. characteristic parameters' number of the output layer is 6, and the number of samples is K. Since the data range of the feature parameter contains negative numbers, we choose the tansig function as the transfer function of the hidden layer. We select the adaptive gradient descent method (Levenberg-Marquardt algorithm) as the training method. The algorithm is characterized by a large memory requirement, a faster convergence speed. It is suitable for a network structure with many neurons and few layers. The loss function chooses the Mean Square Error function (MSE), because MSE is more suitable for neural networks for nonlinear fitting.

As for H-model, there are 24 characteristic parameters and L samples in the input layer. From formulas (7) and (8), $\mathbf{P}_{3\times \mathrm{L}}$ only affects the linear relationship during training, and what we invert is the non-linear mapping relationship. After normalization, $\mathbf{P}_{3\times \mathrm{L}}$ becomes invalid parameters. Due to the reduction of the valid characteristic parameters of the output layer and the reduction of the complexity of the network, the number of neurons in the hidden layer is taken as 200. The training function is the Levenberg-Marquardt algorithm, the hidden layer transfer function is the tansig function, and the loss function is MSE.

Figure 3 shows the convergence process of the E-model and H-model, the abscissa is the number of iterations, and the ordinate is MSE value between the positioning of the models and the label set. We observe that models are approaching the ideal models from the tenth iteration, and the convergence speed of the neural network fitting process is very rapid. In the positioning area with

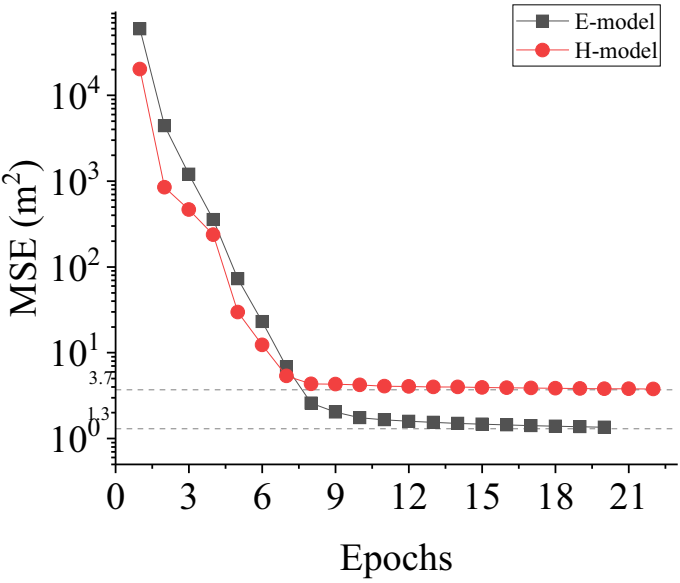

Fig. 3. Convergence processes of E-model and H-model.

a volume of 3000 m^3, MSE eventually tends to 1.3 and 3.7. All of these indicate that models trained by BP neural network has nicer precision and robustness.

4.2 Positioning Method Combining E-Model and H-Model

We measure the electric field data and magnetic field data generated by the electric dipole source at $\mathbf{r}_{test}$ [12], and perform normalization processing to obtain $\mathbf{U}_{test}$ and $\mathbf{H}_{test}$. Input $\mathbf{U}_{test}$ and $\mathbf{H}_{test}$ into E-model and H-model to find the positioning ($\mathbf{r}_{\mathrm{E}}$ and $\mathbf{r}_{\mathrm{H}}$).

Configure the weight factors vectors (α and β) of the E-model and the H-model based on the strength of the interference intensity of $\mathbf{E}_{\mathrm{K}}$ and $\mathbf{M}_{\mathrm{L}}$ in all sub-areas. The final positioning output of the positioning model(E-H-model) that combines the E-model and the H-model is $\mathbf{r}_{\mathrm{EH}} = \alpha \bullet \mathbf{r}_{\mathrm{E}} + \beta \bullet \mathbf{r}_{\mathrm{H}}$.

Figure 4 shows a flowchart of the E-H-model positioning method.

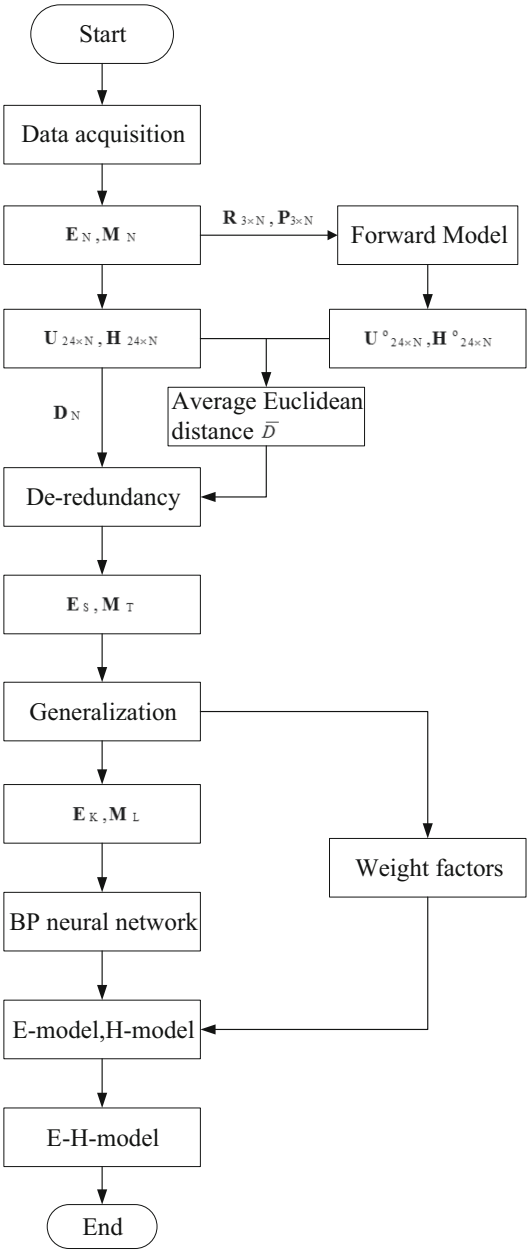

Fig. 4. Overall flow of the E-H-model positioning method.

5 Simulation

We use the three inversion models to positioning scattered targets distributed in the plane (z = 15), and visualize the positioning results. As shown in the Fig. 5, we set the a interference with strong magnetic disturbance and weak electrical disturbance at the coordinates (30, 10, 15). Another interference source with strong electric disturbance and weak magnetic disturbance is placed at the coordinate (−30, 10, 15).

E-model, H-model and E-H-model respectively locate the plane (z = 15) in the underwater environment of Fig. 5, and the positioning results are as Fig. 6, Fig. 7 and Fig. 8.

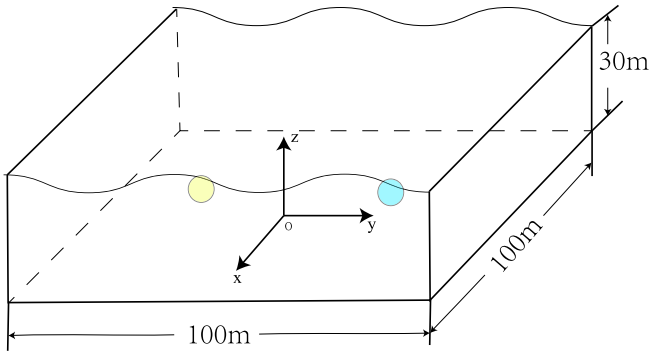

Fig. 5. Distribution of interference sources.

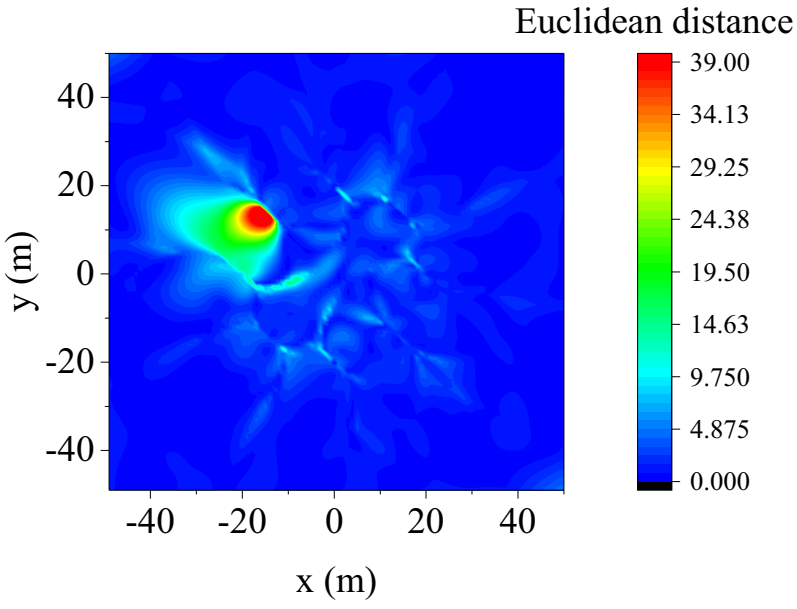

Fig. 6. E-model positioning.

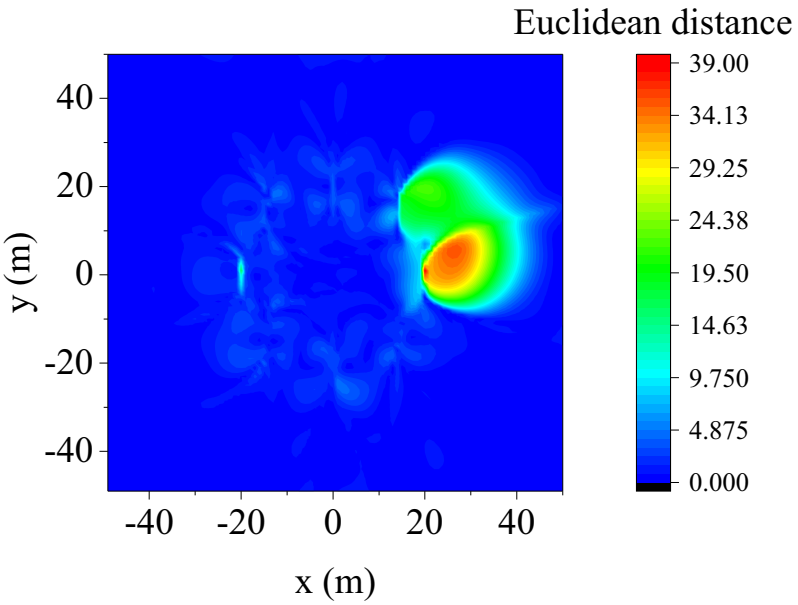

Fig. 7. H-model positioning.

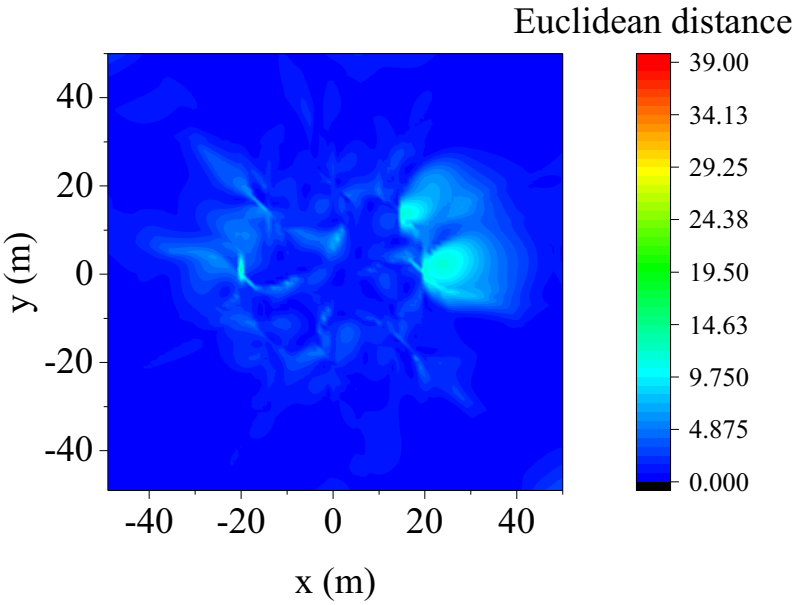

Fig. 8. E-H-model positioning.

In Fig. 6, Fig. 7 and Fig. 8, The axis of abscissa and ordinate indicates the position of the targets in the z = 15 plane. The color map bar represents Euclidean distance (absolute error) between model positioning and target's location.

The positioning error of E-model and H-model is kept within 1 m in the sub-areas without interference. Which indicates that the positioning model trained by the BP neural network has high positioning accuracy. E-H-model reduces the positioning error of E-model in the sub-areas ($x \in (-10, -40)$, $y \in (0, 20)$), reduces the positioning error of H-model in the sub-areas ($x \in (10, 40)$, $y \in (-10, 20)$), and reduces the influence of interference in all sub-areas. These results show that the E-H-model maintains high-precision positioning ability in the sub-areas with greater interference, and improves the anti-interference ability.

We fix the abscissa, and find the Root Mean Square Error (RMSE) of the Euclidean distance values of the column coordinates. The RMSE curves of the E-H-model, E-model, and H-model is drawn in Fig. 9.

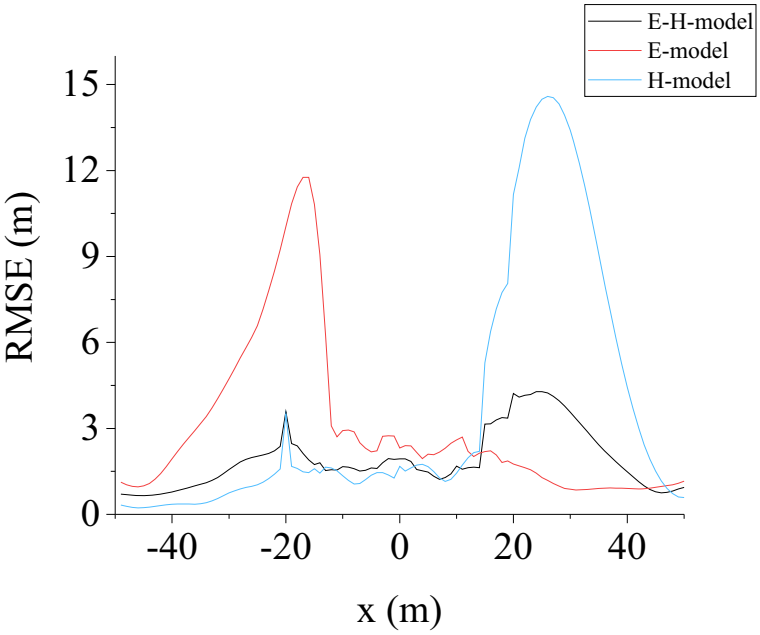

Fig. 9. Comparison of RMSE.

The larger the RMSE value, the larger the positioning error of the abscissa [13,14]. Obviously, the E-model curve is affected by electrical interference ($x = -30$), the H-model curve is affected by magnetic interference ($x = 30$), while the E-H-model curve minimizes these two interferences.

6 Conclusion

This paper applies BP neural network to train E-model and H-model, and proposes a passive electromagnetic field positioning method in underwater 3-D space. This method uses E-model and H-model to ensure positioning accuracy, and adaptively reduces the training samples with larger interference through weight factors. Experiments show that this method overcomes the problem that the E-model and H-model are greatly affected by interference, and reduces the error caused by underwater interference. This method can quickly fit underwater scenes and combine theoretical models with real scenes. It means that passive electromagnetic field positioning methods may no longer be limited to theoretical models. Applying this technology to real scenes is the main directions for deep exploration and improvement.

References

1. Jin, B., Xu, X., Zhu, Y., et al.: Single-source aided semi-autonomous passive location for correcting the position of an underwater vehicle. IEEE Sens. J. **19**(9), 3267–3275 (2019)
2. Wang, J., Li, B.: Electromagnetic fields generated above a shallow sea by a submerged horizontal electric dipole. IEEE Trans. Antennas Propag. **65**(5), 2707–2712 (2017)
3. Panyukov, A.V., Kandelousi, M.S.: Inverse problem for an electrical dipole and the lightning location passive monitoring system. In: Electric Field, pp. 283–300 (2018)
4. Pasku, V., De Angelis, A., De Angelis, G., et al.: Magnetic field-based positioning systems. IEEE Commun. Surv. Tutor. **19**(3), 2003–2017 (2017)
5. Pasku, V., De Angelis, A., Dionigi, M., et al.: A positioning system based on low-frequency magnetic fields. IEEE Trans. Ind. Electron. **63**(4), 2457–2468 (2015)
6. Shoaib, H.S.: Electromagnetic field analysis of a vertical magnetic dipole antenna in planar multi-layered media. IETE Tech. Rev. **38**, 1–8 (2020)
7. Fu, B., Kirchbuchner, F., von Wilmsdorff, J., Grosse-Puppendahl, T., Braun, A., Kuijper, A.: Performing indoor localization with electric potential sensing. J. Ambient Intell. Humaniz. Comput. **10**(2), 731–746 (2018). https://doi.org/10.1007/s12652-018-0879-z
8. Kraichman, M.B.: Handbook of Electromagnetic Propagation in Conducting Media, 1st edn. Headquarters Naval Material Command. University of Illinois at Urbana-Champaign (1970)
9. Zhang, M., Cai, W.: Multi-AUV aided cooperative 3D-localization for underwater sensor networks. Recent Adv. Electr. Electron. Eng. **13**(1), 80–90 (2020)
10. Jiang, J., Zhang, J., Zhang, L., et al.: Passive location resource scheduling based on an improved genetic algorithm. Sensors **18**(7), 2093 (2018)
11. Fang, G., Chen, H., Xie, L.: Precision-improved passive localization method in the underwater multipath environment. In: 2019 IEEE International Conference on Signal Processing. Communications and Computing (ICSPCC), pp. 1–6. IEEE, Dalian (2019)
12. Gao, L., Selleri, S., Battistelli, G., et al.: Passive target detection and tracking from electromagnetic field measurements. Int. J. RF Microw. Comput. Aided Eng. **30**(9), e22321 (2020)

13. Constable, S., Kowalczyk, P., Bloomer, S.: Measuring marine self-potential using an autonomous underwater vehicle. Geophys. J. Int. **215**(1), 49–60 (2018)
14. He, S., Liu, Y., Xiang, J.: A low cost visual positioning system for small scale tracking experiments on underwater vehicles. In: 2020 IEEE 29th International Symposium on Industrial Electronics, pp. 1370–1375. IEEE, Delft (2020)